DENTAL MATERIALS 35 (2019) 389–401

Available online at www.sciencedirect.com

ScienceDirect

journal homepage: www.intl.elsevierhealth.com/journals/dema

Uniaxial/biaxial flexure strengths and elastic properties of resin-composite block materials for CAD/CAM

Beom-Jin Choi[a], *Sungsik Yoon*[b], *Yong-Woon Im*[a,c], *Jung-Hwan Lee*[a,d], *Hyung-Jo Jung*[b], *Hae-Hyoung Lee*[a,d,*]

[a] *Department of Biomaterials Science, College of Dentistry, Dankook University, Cheonan 31116, South Korea*
[b] *Department of Civil and Environmental Engineering, Korea Advanced Institute of Science and Technology, Daejeon 34141, South Korea*
[c] *Department of Dental Laboratory, Kyungdong University, Wonju 26495, South Korea*
[d] *Institute of Tissue Regeneration Engineering, Dankook University, Cheonan 31116, South Korea*

ARTICLE INFO

Article history:
Received 19 August 2018
Received in revised form
18 November 2018
Accepted 28 November 2018

Keywords:
Uniaxial flexure strength
Biaxial flexure strength
Elastic modulus
Poisson's ratio
Resin-composite blocks
CAD/CAM
Digital image correlation

ABSTRACT

Objective. Comparing strengths under different loading conditions provides useful information on the mechanical behaviour of restorative materials under multiaxial masticatory loading in the oral cavity. The aims of this study was to investigate the flexural strengths and the reliability of resin-composite blocks for CAD/CAM by uniaxial and biaxial flexure tests and to compare the elastic properties measured by different methods including digital image correlation (DIC).

Methods. Four resin-composite blocks for CAD/CAM, namely, VE (Vita Enamic), LU (Lava Ultimate), MD (Mazic Duro), and CS (Cerasmart), were investigated. Beam specimens ($4.0 \times 1.4 \times 18.0\,mm^3$) and disks (12–14 mm$\phi \times 1.5$ mm) were prepared to determine the uniaxial (three-point bending) and biaxial (ball-on-ring, BOR) flexural strengths and flexural moduli. A compression test ($8 \times 4 \times 18\,mm^3$) with DIC analysis was utilized to measure the elastic modulus and Poisson's ratio. Data were analysed by a 2-parameter Weibull function and ANOVA with Scheffe's test.

Results. The mean uniaxial and biaxial strengths and Weibull moduli of the specimen groups were as follows: uniaxial VE (140.1 ± 7.0, 24.1), LU (159.1 ± 6.3, 31.5), MD (144.9 ± 13.3, 13.6), and CS (165.4 ± 16.9, 11.2) and biaxial VE (153.6 ± 10.4, 19.0), LU (231.0 ± 29.3, 9.7), MD (148.9 ± 23.8, 7.4), and CS (249.7 ± 22.4, 13.8). Although the ranking of both sets of strength data remained unchanged, the strength reliability was significantly affected by the loading; the Weibull moduli of the specimens decreased when they were subjected to biaxial tests (except for that of CS). The elastic modulus values of the materials varied significantly under the different test loadings, although they were in the same order regardless of the test method: VE > >LU ≈ MD > CS. The DIC technique yielded elastic moduli that were in good agreement with those measured by the uniaxial flexure test.

Significance. The flexural strength, reliability, and elastic modulus of resin-composite block materials differed with the uniaxial and biaxial flexural loading and the test method. The

* *Corresponding author at*: Department of Biomaterials Science, College of Dentistry, Dankook University, 119, Dandae-ro, Cheonan-si, 31116, South Korea.
E-mail address: haelee@dku.edu (H.-H. Lee).
https://doi.org/10.1016/j.dental.2018.11.032

different behaviours under both loadings should be considered in the evaluation of the mechanical performance of those materials.

1. Introduction

Indirect composite resin materials have become a target of great interest in the field of contemporary dental practice, as these materials avoid the various negative effects of direct composite restoration, such as polymerization shrinkage and insufficient degrees of polymerization. The initial version of the indirect composite resin was supplied in a similar form as is used for conventional resin and then subjected to light-curing and additional heat and pressure polymerization processes extraorally to afford so-called artisanal or hand-built composite restorations [1]. However, recently, newer machinable resin-composite block (RCB) materials associated with newer polymerization modes and innovative compositions were developed and have grown in popularity in the market [2]. The transition to these newer materials is associated with the recent explosive growth of dental computer-aided design and manufacturing (CAD/CAM) technology. Currently, indirect restorative materials of this type are classified as chairside RCB materials for dental CAD/CAM systems [3,4]. Most of these materials, such as Lava Ultimate, Cerasmart, and Mazic Duro, consist of bisphenol A-glycidyl methacrylate (Bis-GMA) or urethane dimethacrylate (UDMA) matrices and nanosized silica or silica–zirconia clusters. The other type of materials, such as Vita Enamic, are so-called PICN (polymer-infiltrated-ceramic-network) materials, and they contain feldspar ceramic fillers and an acrylic polymer network [5,6]. These RCBs are cured with an industrial polymerization process under high pressure and temperature and are supplied in the form of rectangular blocks for CAD/CAM [2].

Information on the mechanical properties of newer restorative materials is of great importance to researchers and clinicians because the bulk fracture of the composite resin and CAD/CAM restorations has been reported as the major cause of failure [7,8]. The flexural strength of restorative or prosthetic materials has been most commonly evaluated with uniaxial three- or four-point flexure tests of rectangular beams specimens [9]. International standards for flexural testing of dental resin composites (ISO 4049), ceramics (ISO 6872), and denture base polymers (ISO 20795) demand the specimens have a sufficient length and optimum depth to allow a span-to-depth ratio $\geq$10. However, the commercially available RCB blocks are only supplied in small dimensions with their applications limited to single-unit restorations [10]. Therefore, flexural testing of these materials should be conducted in a miniaturized flexural testing apparatus and analogously sized specimens. However, a large discrepancy in the flexural strengths of the RCBs was found in previous studies, which resulted from specimen dimensions of 1–1.2 $\times$ 4 $\times$ 14 mm^3 (height $\times$ width $\times$ length) with a 10- to12-mm support span [11–14] (Fig. S1). These results can lead to incorrect determinations of the mechanical performance and predictions of their clinical performance. Therefore, more studies are needed to determine reliable strength values and the associated data for these materials.

Another way to determine the flexural properties for specimens with specific size limits, such as CAD/CAM blocks, is a biaxial flexural test using disk or rectangular plate specimens [10]. Moreover, due to the multiaxial loading that occurs during mastication, strength tests under different loading configurations can be helpful for elucidating the relevant properties of dental restorative materials [15,16]. Using an appropriate specimen size for biaxial flexure tests would also be advantageous for simulating the mechanical behaviour of dental restorations in terms of the dimensions of the biaxial specimens, which are similar to natural teeth. [17,18]. Biaxial flexural strength (BFS) tests are also advantageous for avoiding premature failure from edge flaws or cracks parallel to the loading direction, which results in an increased defect detectability for loading areas compared with that of uniaxial flexure loading [19,20]. Therefore, although some uncertainty remains in the stress calculation, biaxial flexure tests have been applied to brittle materials with a wide variety of loading configurations such as piston-on-three-ball (P3B), ring-on-ring (ROR), and ball-on-ring (BOR) [21–25]. However, the piston-on-three-ball test has been criticized for producing nonuniform stress under the piston with a greater strain than predicted, although this test can allow the slight warpage of plate specimens [21]. In the ROR loading scheme, a disk specimen is supported by a ring and loaded with a coaxial loading ring, and this method has also been criticized for stress magnification under the loading ring. Instead, Shetty et al. assumed that the BOR test scheme can generate a more precisely controlled biaxial stress with a simple testing apparatus. [20,21]. Recently, a ball-on-3-ball (B3B) biaxial loading scheme was introduced to test the strength of ceramics, and Wendler et al. reported the biaxial strength for dental CAD/CAM restorative materials using the B3B scheme [10,19]. Among the various biaxial flexure test methods, however, only the P3B test has been adopted by international standards for dental ceramics (ISO 6872) since it was initially approved by the ASTM F394. Therefore, many studies have reported BFS data for dental materials using the P3B test [26]. However, little has been reported using the BOR scheme for biaxial strength testing of dental materials, including resin-composite CAD/CAM block materials.

Generally, dental restorations with a high elastic modulus are desirable to withstand a high occlusal force in oral environments without permanent deformation. On the other hand, mismatches in elastic properties between restoration materials and tooth structure may cause stress concentration at the interfaces, resulting in debonding or failure of the dental adhesive joint [27,28]. Thus, the elastic properties (elastic modulus and Poisson's ratio) are important for predicting the mechan-

Table 1 – Information on dental CAD-CAM resin-ceramic block materials tested.

Material (Manufacturer)	Group	Shade/block	Lot no.	Type (filler content)[a]
Vita Enamic (VITA Zahnfabrik)	VE	2M2-HT/EM-14	N490528	Polymer-infiltrated-ceramic network (86 wt%)
LAVA Ultimate (3 M ESPE)	LU	A1-HT/14L	N42550	Nanoparticle clusters resin-ceramic (80 wt%)
Mazic Duro (Vericom)	MD	A1-HT/14L	MB470101	Nanoparticle resin-ceramic (80 wt%)
Cerasmart (GC Corp.)	CS	A2-HT/14L	1411041	Nanoparticle resin-ceramic (71 wt%)

[a] from manufacturer.

ical behaviour of dental restorations. Those parameters are indispensable in the structural design and finite element analysis of dental restorations or prostheses [29]. A number of studies have reported the elastic properties of various dental materials [14,30–32]. The static elastic modulus is usually determined from the initial tangent line of the stress–strain curve during the uniaxial [7,31,33] or biaxial [34,35] flexure tests. Nondestructive resonant methods have also been used to determine the dynamic elastic properties of dental resin composites [4,32,36]. Each method has its own advantages and disadvantages; however, the static modulus values were always lower than the dynamic modulus values by approximately 20–50% [32,33,37].

An effective optical technique for detecting surface deformation has been employed to measure the elastic properties of various materials and structures, and this technique is known as digital image correlation (DIC). The main advantages of DIC are related to its accuracy, simplicity, and cost-effectiveness, especially in civil engineering fields [38–40]. DIC techniques have been extended to investigating material properties of various types of materials, including biomaterials and dentin [41–43]. This technique has also been utilized to measure the polymer shrinkage of dental composite resins [44,45]. However, to date, investigations of the bulk mechanical properties of restorative materials using this technique have been rare.

In the present study, the flexural strengths of various RCB materials for CAD/CAM were measured by uniaxial (three-point flexure) and biaxial (BOR) tests, and the strength reliability and possible effects of specimen size were explored with Weibull statistics. The elastic moduli obtained from the uniaxial and biaxial flexure tests were compared with those independently determined by the DIC technique during the compressive test. The null hypothesis to be tested was that the flexural and elastic properties of resin-composite CAD/CAM block materials determined by these measurement methods are not different. Secondary and backscattering electron microscopy were used to observe the microstructural differences of the RCB materials.

2. Materials and methods

2.1. *Preparation of specimens for uniaxial and biaxial flexural tests*

The four RCB materials for CAD/CAM investigated are summarized in Table 1. The respective as-received RCBs were sectioned into rectangular bar specimens with nominal sizes of $1.4 \times 4 \times 18\,mm^3$ (depth × width × height) for uniaxial flexural testing. The sectioning of all specimens was performed using a high-speed precision cutting machine (Accutom-50, Struers, Ballerup, Denmark) with a metal-bonded diamond cut-off wheel (M0D13) at a wheel speed of 3800 rpm and feed speed of 0.05 mm/s under cooling with large amounts of water. The specimens were ground flat using P1200-P2400 SiC paper (Struers[SE1]), and further surfaces on the tension side were sequentially polished with 6, 3, and 1 μm diamond slurries (Struers). The edges of the bar specimens were chamfered with P2400 SiC paper.

The disk specimens for biaxial flexural testing were obtained by slicing cylindrical RCBs, which were machined from the as-received blocks by a bench lathe (DML 210, Dajoo Hi-Tech, Korea) with a carbide turning tool. The slicing procedures were performed using the above mentioned cutting machine, and the surfaces of the disks were finished with the same procedure as was used for the bar specimens. The nominal size of the prepared disks was 14.0 mm in diameter and 1.5 mm in thickness, except for VE (12 mm in diameter), due to the limitations in the size of the supplied material. The specimen surfaces were also finished with the abovementioned protocol followed by fine diamond polishing of the tension surface. The opposing faces of the prepared specimens were parallel within 0.02 mm. The diameter (±0.01 mm) and width/thickness (±0.001 mm) of specimens were measured at three different places and averaged using digital callipers (Mitutoyo, Japan) and a stand-type digital dial gauge (ID-C 112, Mitutoyo, Japan), respectively. Fig. 1 shows the as-received RCBs and the prepared specimens for uniaxial and biaxial flexure tests.

The surface roughness values (ten-point mean roughness, R_z) of the diamond-polished surfaces of both bar and disk specimens were approximately $0.3 \pm 0.01\,\mu m$ as measured from the selected specimens (n = 6) using a roughness tester (SJ-400, Mitutoyo, Japan). All specimens were stored in distilled water at 37 °C for 48 h prior to uniaxial and biaxial flexural testing.

2.2. *Uniaxial flexural strength and flexural modulus*

The uniaxial flexural strength (UFS) and modulus were determined using a three-point bending test at a 14-mm span length. The bar specimens were loaded at a constant crosshead speed of 1.0 mm/min in a universal testing machine (Instron 3344, Norwood, MA, USA) with an apparatus consisting of three rods (2 mm in diameter) (Fig. 1(a)). The ultimate flexural stress (σ_{3PF}) and flexural modulus (E_{UF}) were calculated at the maximum flexure/fracture load on the load-displacement curve using the following equations:

$$\sigma_{3PF} = 3PL/2bd^2 \quad (1)$$

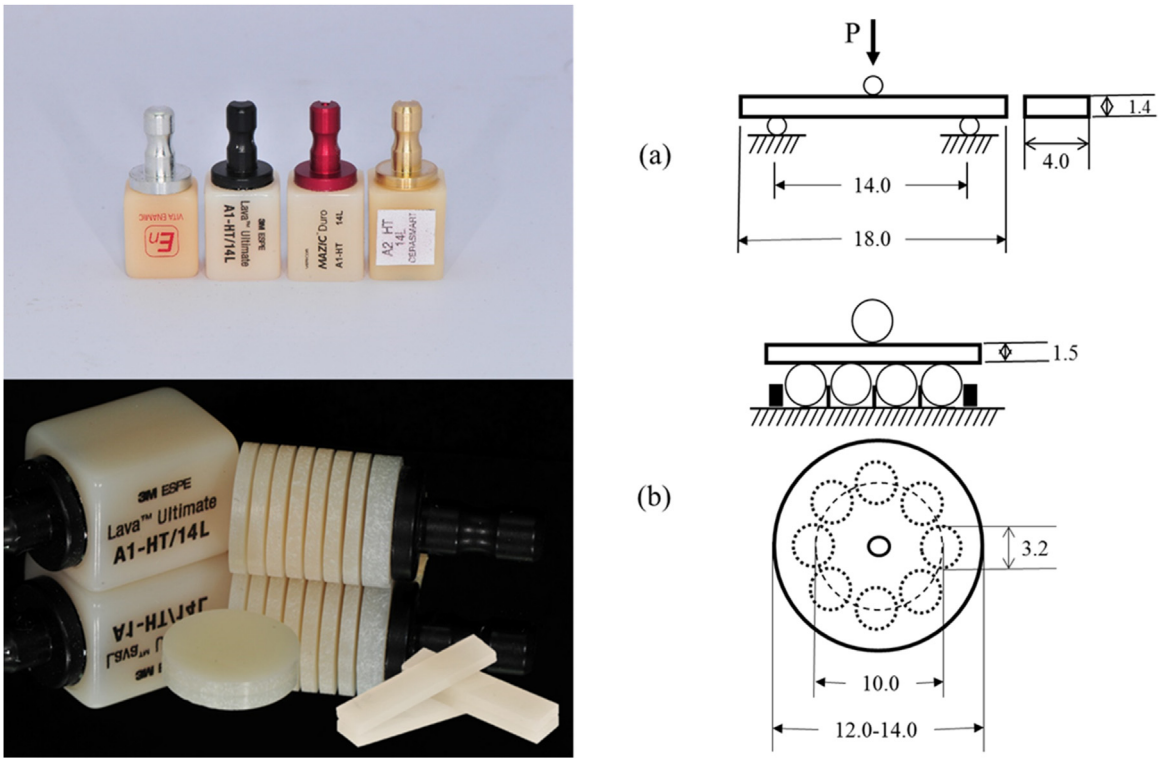

Fig. 1 – RCBs for CAD/CAM and the three-point uniaxial flexure (a) and BOR biaxial flexure (b) testing setups.

$$E_{UF} = L^3 m / 4bd^3 \quad (2)$$

where P is the maximum flexure load (N), L is the length of the support span, b is the width of the specimen (mm), d is the height of the specimen (mm), and m is the slope of the modulus line (N/mm) constructed along the linear portion of the stress-strain curve using the Bluehill software [46]. A total of 30 specimens were tested for each group, except for MD (n = 24).

2.3. *Biaxial flexural strength and flexural modulus*

The BFS of each disk specimen was determined by a BOR test. The tension side of the disk was supported on a ring (5 mm in radius) consisting of eight hardened steel ball bearings aligned in a circular guide to permit free motion and minimize frictional stresses with the disk [20,47]. Then, the disk samples were centrally loaded with a ball-end plunger at the centre of the testing apparatus at a cross-head speed of 1.0 mm/min (Fig. 1(b)). All supporting and loading balls were 3.2 mm in diameter.

The BFS (σ_{BOR}) was calculated by the following equation proposed by Shetty et al. [21] and based on the solution by Kirstein and Woolley [48]:

$$\sigma_{BOR} = \frac{3P(1+\upsilon)}{4\pi t^2}\left[1 + 2\ln\frac{a}{b} + \frac{(1-\upsilon)}{(1+\upsilon)}\left(1 - \frac{b}{2a^2}\right)\frac{a^2}{r^2}\right] \quad (3)$$

where P is the maximum load at failure, υ is Poisson's ratio, a is the radius of the supporting circle (5 mm), r is the radius of the disk sample, t is the thickness of the disk, and b is the radius of the region of uniform loading at the centre. The value of b indicates the effective radius of contact between the loading ball and the specimen, and the contact radius (z) can be calculated using Hertz's elastic contact theory [20,49]:

$$z = \left[\frac{3Pr}{4}\left(\frac{1-\upsilon_1^2}{E_1} + \frac{1-\upsilon_2^2}{E_2}\right)\right]^{1/3} \quad (4)$$

where E_1 (ν_1) and E_2 (ν_2) are the elastic modulus (Poisson's ratio) of the specimen and the loading ball (E_2 = 200 GPa, and ν_2 = 0.29), respectively [49]. For $z < 1.724t$, σ_{BOR} can be calculated by using an equivalent radius $\bar{b}$ in the following expression proposed by Westergaard [50]:

$$\bar{b} = \sqrt{(1.6z^2 + t^2)} - 0.675t \quad (5)$$

The contact radius or equivalent radius is dependent on the elastic properties of the materials and the flexure load. In this study, the BOR strength of the materials was determined using their respective z and $\bar{b}$ values calculated from Eqs. (4) and (5). The Poisson's ratio of each material for calculating its biaxial strength was obtained from the subsequent DIC test (Table 3). Twenty disk specimens were tested for each group (n = 20). No compliant layer between the balls and disks was used in this study.

The biaxial flexural modulus (E_{BF}) was calculated using the following equation [34,35]:

$$E_{BF} = \frac{\beta P a^2}{\omega h^3} \quad (6)$$

Table 2 – Mean uniaxial flexural strength (3-point flexure test, UFS) and biaxial flexural strength (ball-on-ring test, BFS) values for the investigated materials, and their Weibull moduli (*m* values) and characteristic strengths (σ_0 values) with 95% confidence interval.

Material	Uniaxial flexure strength (MPa)	Biaxial flexure strength (MPa)	Uniaxial flexure		Biaxial flexure	
			σ_0 (95% CI)	*m* (95% CI)	σ_0 (95% CI)	*m* (95% CI)
VE	140.1 (7.0)^{Aa}	153.6 (10.4)^{Ab}	143.2 (141.0–145.5)	24.1 (18.2–31.9)	158.2 (154.4–162.0)	19.0 (13.4–27.1)
LU	159.1 (6.3)^{Ba}	231.0 (29.3)^{Bb}	161.8 (159.8–163.9)	31.5 (24.3–40.8)	242.5 (230.7–254.9)	9.7 (6.9–13.5)
MD	144.9 (13.3)^{Aa}	148.9 (23.8)^{Aa}	150.3 (145.3–155.4)	13.6 (10.2–18.1)	158.1 (148.5–168.3)	7.6 (5.5–10.6)
CS	165.4 (16.9)^{Ba}	249.7 (22.4)^{Bb}	172.8 (167.1–178.7)	11.2 (8.7–14.9)	258.8 (249.4–268.5)	13.8 (10.2–18.6)

Same superscripts in column (upper case) and in row (lower case) indicates statistically identical groups at $p < 0.05$.

Table 3 – Mean elastic moduli (GPa) measured using four different testing methods and Poisson's ratios of the materials.

Test method	Vita Enamic	Lava Ultimate	Mazic Duro	Cerasmart
Uniaxial flexure (E_{UF})	24.54 (0.29)^{Ab}	10.86 (0.13)^{Ba}	10.70 (0.26)^{Ba}	7.64 (0.14)^{Cb}
Biaxial flexure (E_{BF})	4.38 (0.17)^{Ad}	3.23 (0.19)^{Bc}	2.88 (0.14)^{Cc}	2.65 (0.05)^{Dd}
Compression (E_{COM})	11.18 (0.33)^{Ac}	7.44 (0.08)^{Bb}	7.45 (0.21)^{Bb}	5.63 (0.05)^{Cc}
DIC (E_{DIC})	26.45 (1.74)^{Aa}	11.14 (0.75)^{Ba}	10.95 (1.04)^{Ba}	7.95 (0.16)^{Ca}
Poisson's ratio	0.277 (0.02)^{A}	0.302 (0.03)^{A}	0.295 (0.01)^{A}	0.306 (0.02)^{A}

Same superscript letters in row (upper case) and column (lower case) indicate statistically identical groups at $p < 0.05$.

where ω is the deflection at centre (mm), h is the thickness of the disk sample and β is the centre deflection function given by:

$$\beta = -0.0642 - 2.1900m^{-3} + \left(0.5687 + 3.254m^{-3}\right)\left(1-\upsilon^2\right) + \left[-0.0379 + 11.0513m^{-3} + \left(0.5223 - 7.8535m^{-3}\right)\left(1-\upsilon^2\right)\right]t^3 \quad (7)$$

where m is the number of equally spaced ball supports and t is the ratio of the support ring radius to the disk radius. In this study, the centre deflection and load for calculating E_{BF} were selected from the linear portion of the load-displacement curve of the specimens.

The microstructures of the polished and fractured surfaces of the specimens were observed by secondary and back scattering electron microscopy using a scanning electron microscope (SEM-3000H, Hitachi, Japan) after gold sputtering.

2.4. *Weibull analysis*

The UFS/BFS data were evaluated with a two-parameter Weibull distribution function [51]:

$$P_f = 1 - \exp\left[-\left(\frac{\sigma}{\sigma_0}\right)\right]^m \quad (8)$$

where P_f is the cumulative probability of failure, σ is the fracture stress, σ_0 is the characteristic parameter corresponding to a fracture probability of 63.2%, and m is the Weibull modulus. The Weibull modulus (m) and characteristic strength (σ_0) with confidence intervals of 95% were obtained using commercial software (Weibull++, version 6.0, ReliaSoft, USA) based on the median ranks method and rank regression on X (RRX).

2.5. *Elastic properties measured by digital image contrast*

The RCBs were cut into rectangular beam specimens with a nominal size of 4 × 8 × 18 mm (width × depth × height). Speckle patterns for DIC analysis were prepared on the side surfaces of the specimens. Because image matching algorithms are based on grey-intensity distributions, the randomness of the grey-intensity is essential for improving the accuracy of the DIC results [40,43]. Therefore, speckle patterns were generated on the surface at a low volume fraction (35–40%) by spraying white and black paint using an airbrush (Harder & Steenbeck Co.) with a 0.2-mm air nozzle. The DIC specimens with speckle patterns were vertically loaded under uniaxial compression on a material testing machine (Instron 5966) at a speed of 0.1 mm/min after correction of machine compliance. Compressive loading was continued until the samples began to yield from the stress–strain relation, and the speckle patterns were acquired using the DIC experimental setup equipped with a digital single reflex lens (DSRL) camera (7d Mark II, Cannon) (Fig. 2). During the compressive loading, images of the speckle patterns were taken at an interval of 1000 N from the linear portion of the stress–strain curve. For image correlation, regions of interest (ROIs) of 1000 × 1000 pixels (approx. 5.76 mm^2) selected from the images were stored in an 8-bit format as reference and deformed images (Fig. 2). The motion vector can be measured within the ROI based on the similarity to the greyscale of the stored image (0–255), and this technique was conducted with full-field two-dimensional (2D)-DIC algorithm developed in MATLAB (R2014a, MathWorks) [40,52] to calculate the horizontal and vertical strains for determining the elastic modulus and Poisson's ratio (Fig. 2). In this study, four specimens of each material were evaluated by DIC analysis. In addition, the compressive elastic modulus values without a DIC of the specimens were calculated from the load-displacement curve of the testing machine data.

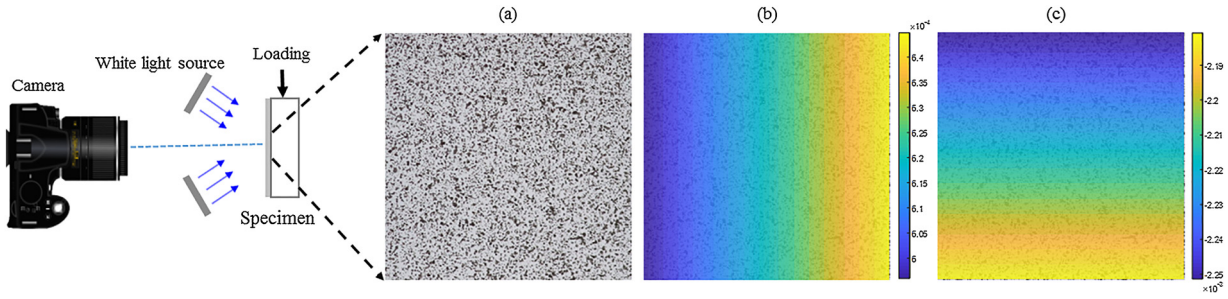

Fig. 2 – Test setup for DIC measurement. (a) Reference image, (b) deformed image overlaid with the horizontal strain field, and (c) deformed image overlaid with the vertical strain field.

2.6. *Data analysis*

Statistical significance was determined by one-way analysis of variance with a post hoc test (Scheffe's test) using Statistical Package for the Social Sciences (SPSS 23.0, Chicago, IL, USA). A p-value < 0.05 was considered statistically significant.

3. Results

Typical stress–strain curves for the uniaxial flexure tests and load–displacement curves for the biaxial flexure tests of the RCB materials are displayed in Fig. 3. Except for VE, the block materials (LU, MD, and CS) exhibited nonlinear behaviour with an elastic limit during the uniaxial flexure tests. However, not all materials showed a plastic region before specimen fracture during the biaxial flexure tests. The mean UFS and BFS values for the resin-composite materials investigated are listed in Table 2. The BFS values of the specimen groups were significantly higher than their UFS counterparts ($p < 0.05$), except for MD. In particular, the mean BFS values of LU and CS (231 and 250 MPa, respectively) were higher up to 45–50% than their UFS values (159 and 165 MPa, respectively). There was no significant difference in the UFS or BFS values between LU and CS or between VE and MD; however, the strengths of LU and CS were significantly higher than those of VE and MD by both measures ($p > 0.05$).

Weibull plots of the UFS and BFS data of all groups are shown in Fig. 4. The Weibull modulus and characteristic strength values with their 95% confidence intervals are summarized in Table 2. For UFS, LU had the highest Weibull modulus ($m = 31.5$) among the RCB materials, which, along with VE ($m = 24.1$), were significantly higher than those of MD and CS. However, except for the value for CS, the overall Weibull moduli were significantly lower based on the BFS results, particularly for UL (from 31.5 to 9.7) and MD (from 13.6 to 7.6). VE showed the highest reliability in biaxial strength among the RCBs. Multiple radiant fracture paths were observed from the centre of the biaxial disks with a positive correlation between the number of fragments and the BFS values for all RCB materials (Fig. 5).

The elastic modulus data for the specimens determined by the four different methods (uniaxial flexure, biaxial flexure, compression, and DIC) along with Poisson's ratio as determined by the DIC method are summarized in Table 3. The elastic moduli of all the materials measured by 3-point flexure strength (E_{UF}) generally were in good agreement with their values determined by DIC (E_{DIC}), followed by E_{COM} and E_{BF}. The E_{BF} values of the RCB materials were considerably lower than their respective E_{UF} and other values. Overall, EN showed significantly higher elastic moduli for all testing methods, followed by LU ≈ MD and CS. The values of Poisson's ratio of the specimens ranged from 0.277 to 0.306, and no significant differences were observed.

Fig. 6 shows the secondary and back scattering electron (BSE) images of the polished surfaces of the four materials. Zirconia particles sparsely dispersed in the ceramic (filler) network of VE were clearly seen as white dots in the BSE image [4,12]. LU shows spherical particles with sizes typically from 1–5 μm clustered with resin and nanoceramic particles, while MD and CS show nanosized particles uniformly dispersed in the resin matrix. The respective characteristic microstructures appeared as the fractured surfaces of materials, and they showed intergranular crack propagations (Fig. 7).

4. Discussion

4.1. *Uniaxial and biaxial flexural strength*

Although there was a positive correlation between the UFS and BFS values of the RCB materials in this study ($r^2 = 0.954$), the discrepancies between both strength values were highly dependent on the resin-composite block material tested. The tested hypothesis was rejected as significantly different flexural strengths and elastic moduli were observed by the different test methods for the RCB materials. Uniaxial three-point bend tests are widely accepted for testing the flexural properties of dental materials over other mechanical testing techniques. However, the flexural strength can be significantly altered by several factors originating from specimen geometry, test configuration, and testing apparatus [53]. Thus, those factors and the quality of the surface finishing have to be taken into account during the evaluation of strength data. There have been contradictory results on the UFS (3-point flexure strength) of RCB materials among previous reports (Fig. S1). One study using a low span-to-depth (S/D) ratio (~5) revealed considerably high flexure strength data for RCBs [14]. Moreover, the flexural strength values vary considerably among the previous reports, although specimen dimensions and test geometries similar to those of the present study were used. Therefore, a new testing protocol should be developed for the

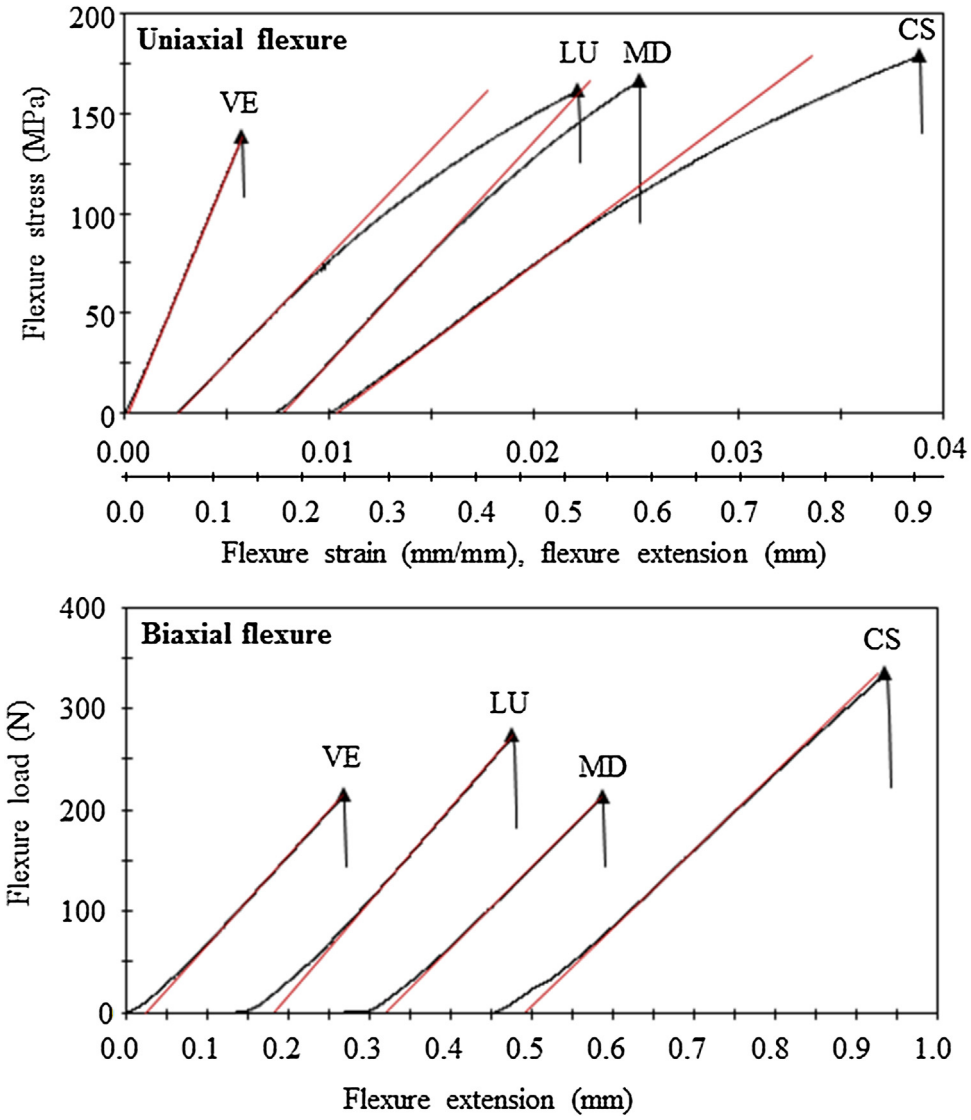

Fig. 3 – Typical stress-strain and load-displacement curves for RCB materials for CAD/CAM. Red lines indicate the modulus lines constructed by software (Bluehill). (For interpretation of the references to colour in this figure legend, the reader is referred to the web version of this article.)

precise and accurate measurement of the flexural properties of RCB materials.

Stress–strain or load–displacement curves under a loading condition provide important information on the material's mechanical behaviour; however, previous papers often omit this diagram. Typical load–displacement curves of the RCBs reveal a distinct difference between uniaxial and biaxial flexure (Fig. 3). Under the uniaxial test configuration of the present study, the specimens (except for VE) generally showed a non-linear deformation before ultimate failure, while they failed within the linear elastic range under biaxial loading. These behaviours of RCBs were generally consistent with the results of light-curing composite resins [18]. A PICN material VE revealed only a linear elastic deformation under both flexure loadings with high stiffness, which must be attributed to the continuous ceramic-network microstructure [4], as shown in Fig. 6. Compared with the uniaxial flexure test results (50–70 N), the BOR biaxial loading produced high maximum fracture loads (200–400 N) for similar dimensions of specimens that were closer to the occlusal force in natural dentition [54]. Thus, although the fracture energy or stress is dependent on specimen's geometry, the biaxial flexure test may offer clinically relevant fracture resistance values for those materials. A high positive correlation between the number of fragments and the biaxial strength value was demonstrated for overall RCB materials (Fig. 5). This trend (for VE and UL) appeared more clearly in the BOR testing than that observed in the 3PBS testing of a previous study [55]. The multiple fragmentations in the biaxial disks result from the high-strain energy stored during loading [10,56].

Biaxial flexure tests were originally developed for brittle ceramic or glassy materials, and solutions for the BFS were based on a linear elastic equation by Kirstein and Woolley [48]. For the use of this equation to be valid, during the biaxial test,

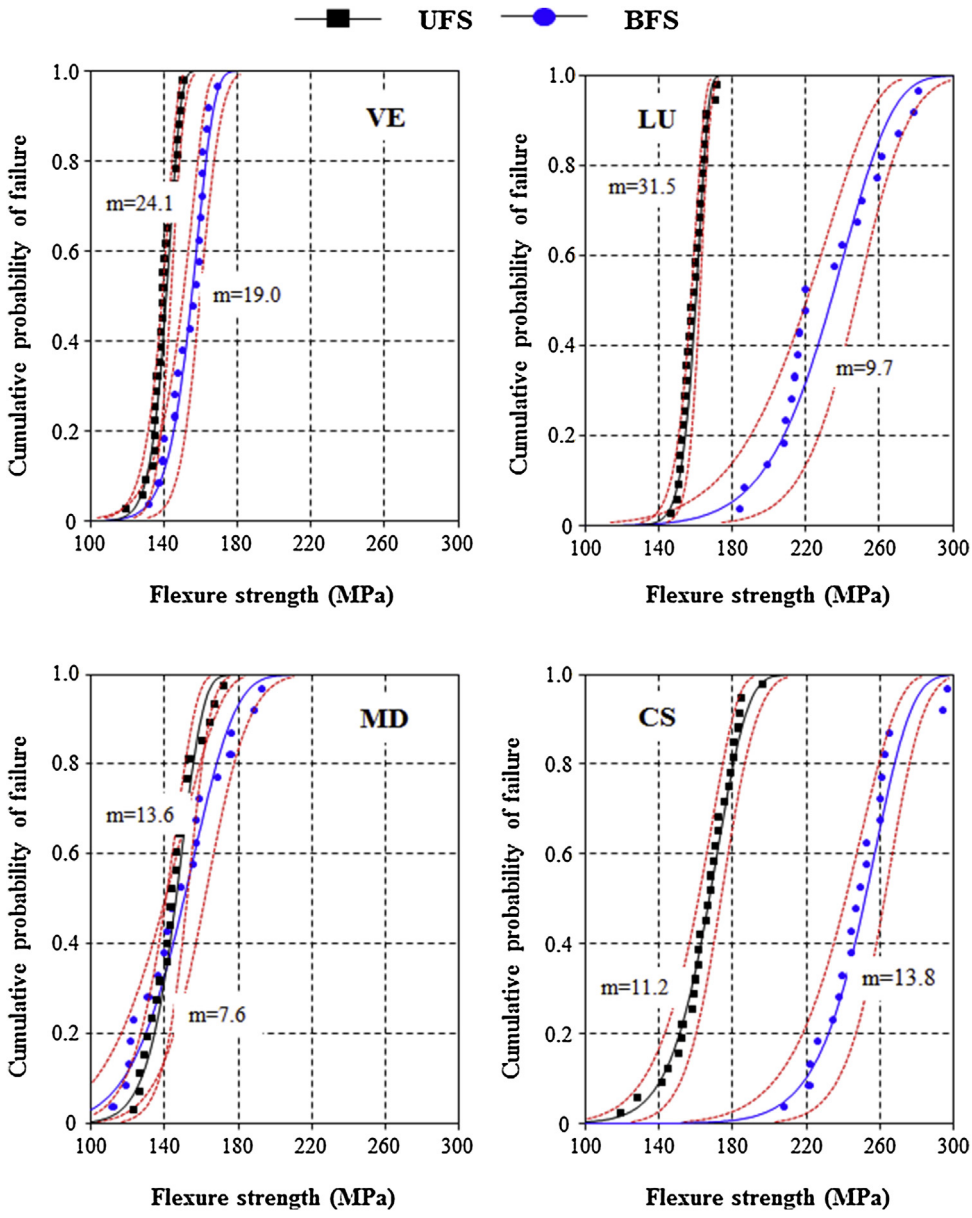

Fig. 4 – Weibull plots for uniaxial and biaxial strengths of the materials.

the deflection of the specimen at its centre must not exceed one-half of the specimen thickness [57], i.e., $\omega < 0.5t$. Otherwise, the true stress cannot be solved by the linear elastic solution due to a substantial membrane stress effect [58]. Kao et al. (1971) demonstrated that significant stress magnification during biaxial loading can develop at the centre of the specimen when $\omega > 0.5\,t$ [58]. In the present study, the ω/t values of all samples were well below <0.5, but the overall strength typically increased with increasing ω/t values (Fig. S2). This result indicates that for materials with a low elastic modulus and high deflection, biaxial flexure tests should be applied cautiously.

To calculate the biaxial strength, all parameters for the equations should be replaced with accurate values. In the case of ceramic materials, $\bar{b}$ was assumed to be t/3 in a typical BOR test setup [20,21]. However, $\bar{b}$ can deviate from t/3 for materials with a low modulus due to the large stiffness difference with the loading ball [49]. Here, we inputted the $\bar{b}$ value calculated for each individual specimen to determine the BFS. The relation between the z and $\bar{b}$ values varied with the applied load, as illustrated for the two typical materials in Fig. S3. The maximum difference between the $\bar{b}$ values of EN (high modulus) and CS (low modulus) was approximately 0.05 mm. However, the systematic error in the BFS values was <4% for the RCBs investigated. Thus, the $\bar{b} = t/3$ assumption for ceramics can be safely used to determine the BOR strength of the RCB materials. In previous studies, however, the z value in the calculation of the equivalent radius ($\bar{b}$) using Eq. (5) was often taken as the radius of the loading ball [18,59], not the contact radius (z) between the ball and disk, resulting in a threefold increase in the $\bar{b}$value. The two different $\bar{b}$ values in turn provide substantially different calculated biaxial strengths.

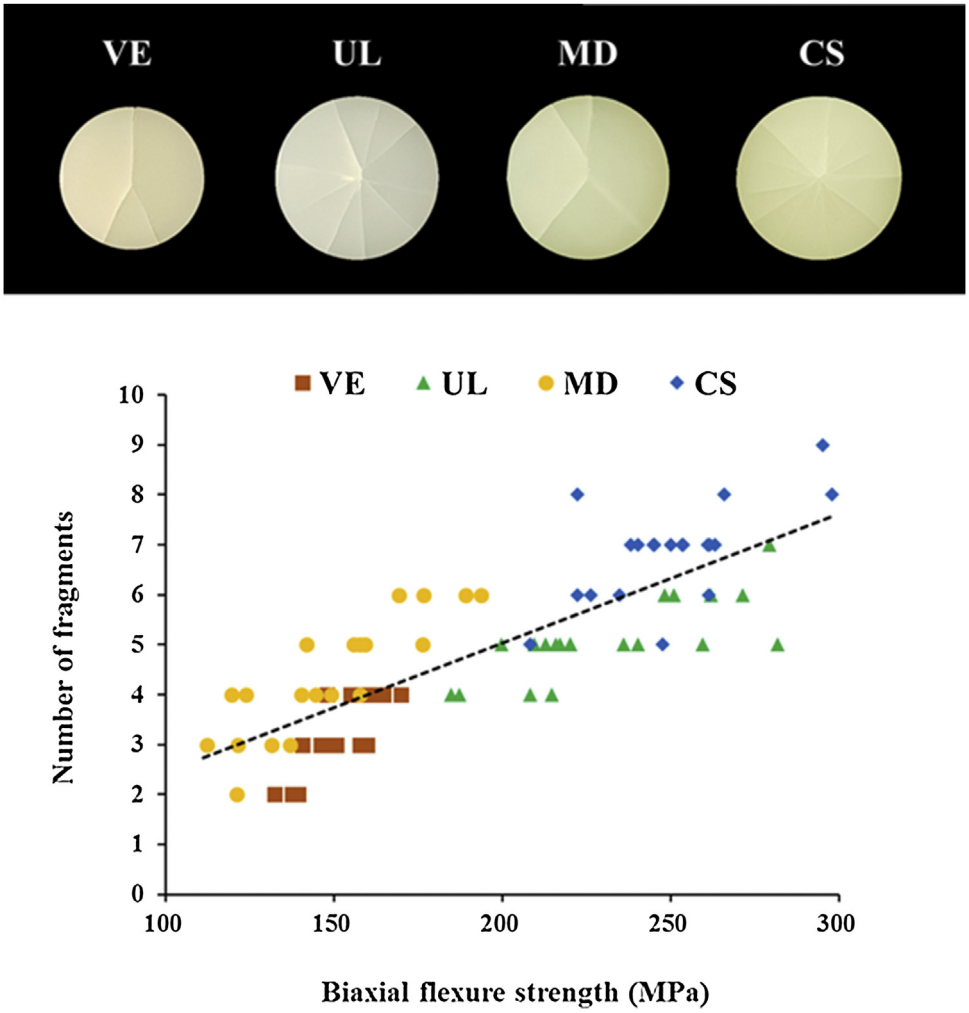

Fig. 5 – Photographs of fractured disks from the BOR biaxial tests and relation between the number of fragment and the BFS of RCB materials.

Weibull analysis provides the strength reliability of the material based on the scattering of the data. The Weibull results showed that the strength reliability of RCBs decreased when they were subjected to the biaxial strength test (except for CS), but the overall effect was substantially dependent on the material (Fig. 4). Previous studies have reported the biaxial strengths of two RCBs (VE and LU) using disks specimens but under different loading configurations: B3B [10,14,55] or P3B [55]. A wide variation exists among the biaxial strength results of those reports; however, their Weibull moduli (m) were generally identical to those in this study, i.e., a higher m value for VE than for LU. VE ranked the most reliable in biaxial strength among the RCBs tested. In the case of light-cured composite resins, however, the m values were higher when they were subjected to the biaxial flexure test rather than in the uniaxial flexure test [17,60,61]. This discrepancy in the strength reliability between RCBs and composite resin materials is probably due to differences in the fabrication process of specimens between factory manufacturing (RCB) and the hand-built method (composite resin) [55].

The size or stress state effect on the strength values originating from the different dimensions of specimens and test geometries has been established by several studies based on the Weibull theory [62,63]. The strength of materials under a certain stress state or specimen size can be scaled with Weibull effective volumes or effective surface areas and can be predicted using the following relation:

$$\frac{\sigma_1}{\sigma_2} = \left(\frac{A_{e2}}{A_{e1}}\right)^{1/m} = \left(\frac{V_{e2}}{V_{e1}}\right)^{1/m} \quad (9)$$

where σ_1 and σ_2 are the mean strengths of each specimen, A_{e1} and A_{e2} are the effective surface areas, A_{e1} and A_{e2} are the effective volumes, and m is the Weibull modulus. The approximation of the effective area and volume for the multiaxial stress state, such as the BOR biaxial flexure test, must involve the integration of multiple theorems, yet no simplified formulas have been developed [64]. Some researchers have introduced the concept of an equivalent stress state and the principle of independent action (PIA criterion) in such analyses to allow comparisons between the two loading configurations [10,65]. We here tried to predict the strength based

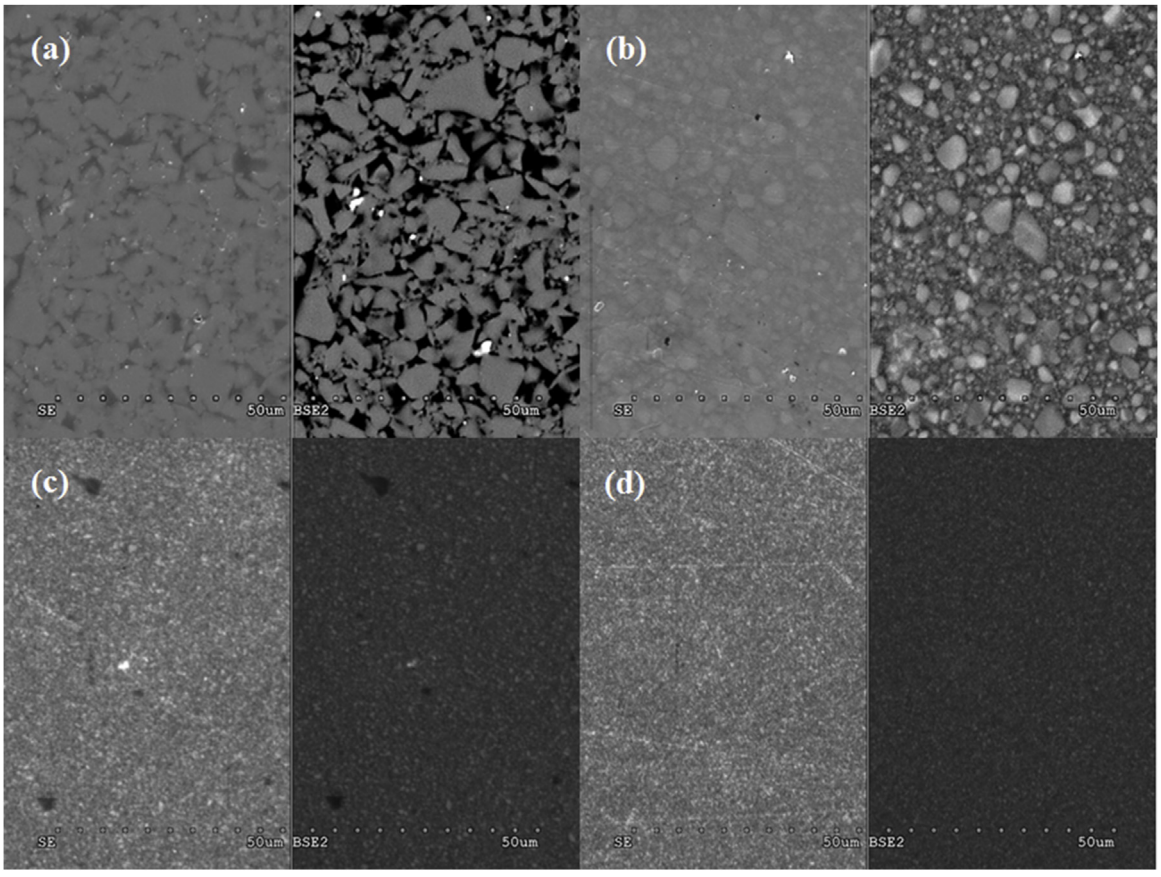

Fig. 6 – Secondary electron (SE) and back scattering images (BSI) of the polished surfaces. (a) VE, (b) LU, (c) MD, and (d) CS.

on the two test geometries using the effective volume formulas for a uniform-pressure-on-ring biaxial loading, which were proposed by Chao and Shetty [62]:

$$V_{eff}^{3PF} = Lbd/2(m+1)^2 \quad (10)$$

$$V_{eff}^{BFS} = \pi r^2 t/2\beta(1+m)^2,\ \beta = 3P(1+3\nu)r^2/8t^2\sigma_{BFS} \quad (11)$$

The effective volume for the uniaxial (V_{eff}^{3PF}) and biaxial flexure (V_{eff}^{BFS}) tests and the predicted strength values based on Eq. (9) are summarized in Table 4. As a result, two materials (VE and MD) showed good agreement in the predictions of BFS from UFS, while the BFS values of the other two materials (UL and CS) were underestimated. These results were generally in good agreement with previous findings [10,63]; which assessed the effect of size in uniaxial tests but underestimated the biaxial stress for ceramics. The reasoning behind this underestimation is unclear, but the imperfect scaling can be mainly explained by factors such as differences in flaw types and distribution and microstructural response in the different specimens and tests. Discrimination of fracture origin by fractography is mandatory to fully elucidate this phenomenon [62,66].

4.2. *Elastic modulus measured by four different test methods*

The elastic moduli of the RCBs investigated in this study fall in the same ranking regardless of the testing method: VE > >LU ≈ MD > CS. Therefore, each set of measurements can be used to detect the differences in the elastic properties of RCB materials. The elastic moduli (E_{DIC}) values determined by DIC were significantly higher than the (E_{COM}) values determined by the load-displacement relation from the mechanical testing machine, particularly for high-stiffness materials (VE). This result indicates that the strain value acquired directly from the displacement curve of specimens is not accurate, probably due to an inadequate compensation of machine compliance [67]. Previous studies have demonstrated that the DIC technique can be used as a substitute for a strain gauge or extensometer in measuring Young's modulus of metals, polymer composites, and biological materials [43,68]. Notably, for all RCBs, the mean E_{DIC} values were in good agreement with their respective E_{UF} values in this study. The elastic modulus values of these materials determined by three-point bend tests in previous studies were comparable to the corresponding E_{UF} values of this study [11–14], although their flexure strength values varied widely. In this regard, a three-point bend test (especially with the S/D ratio of 10) can be a practical guide for determining the elastic modulus of RCBs, although further studies are warranted.

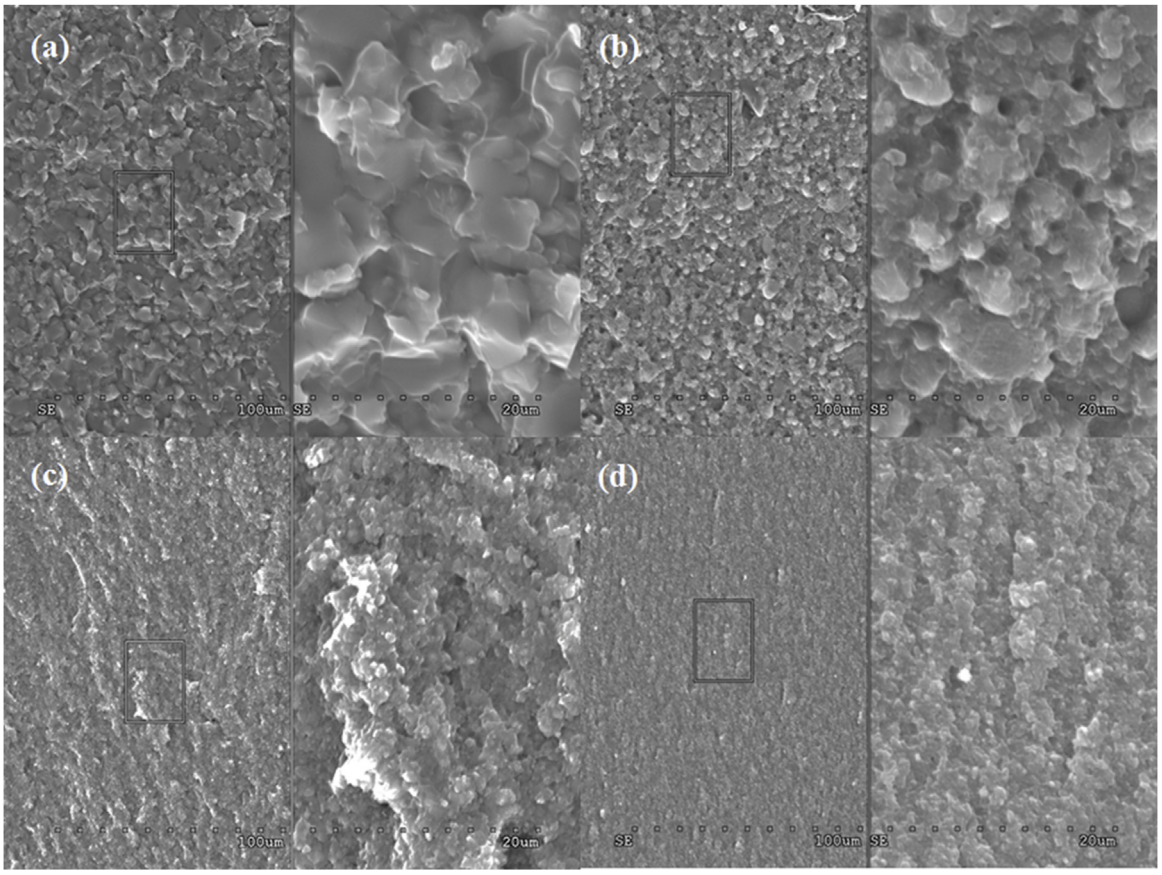

Fig. 7 – Microstructures of the fractured surfaces. Right is the magnified image of the rectangular area on the left. (a) VE, (b) LU, (c) MD, and (d) CS.

Table 4 – Measure and predicted biaxial flexure strength of specimens. Effective volume uniaxial flexure (V_{eff}^{UFS}) and biaxial flexure (V_{eff}^{BFS}).

	V_{eff}^{UFS} (mm^3)	V_{eff}^{BFS}(mm^3)	BFS-measured (MPa)	BFS-predicted (MPa)
VE	0.0622	0.0145	154	149
LU	0.0371	0.0516	231	158
MD	0.1842	0.0746	149	155
CS	0.2632	0.0255	250	204

The elastic modulus (E_{BF}) values of RCBs determined by the BOR biaxial loading were significantly lower than those determined by other methods (uniaxial flexure and compression tests with and without DIC), although for acrylic cements (~2 GPa), no significant differences were found between the elastic modulus values determined by uniaxial and those determined by biaxial flexure tests in previous studies [35]. These results may indicate some uncertainty in the calculation of biaxial modulus using Eq. (5), particularly for materials with a high modulus of elasticity. When measuring with a strain gauge, no differences were found in the elastic modulus values determined by various uniaxial or biaxial tests, even for high-stiffness ceramic materials [62,69]. Therefore, the measurement of elastic modulus using the biaxial flexure test should not be recommended without additional strain measurements.

5. Conclusion

The wide scattering among previous data for RCB materials for CAD/CAM highlights the necessity of valid mechanical tests and interpretation methods. For those materials, the uniaxial (three-point flexure) and biaxial (BOR) flexural strength tests with the measurements of the related elastic properties were conducted in this study to explore the mechanical behaviours and reliabilities under different loading conditions via Weibull analyses. Although the ranking of the strengths by both measurements was the same, the strength reliability significantly differed based on the testing method and materials tested. Therefore, the flexural strength values of the RCB materials should be evaluated under two different loadings. The DIC technique was successfully used to measure the elastic prop-

erties of RCBs. The elastic modulus (E_{DIC}) values determined by DIC were in good agreement with the values (E_{UF}) measured by the three-point flexure test at an S/D ratio of 10, which were higher than those measured by biaxial flexure and compression tests without a strain gauge.

Acknowledgment

This research was supported by Basic Science Research Program (2015R1A2A2A01007567) and Global Research Development Center Program (2018K1A4A3A01064257) through the National Research Foundation funded by the MSIT of Korea. The materials (MD and CS) were kindly donated by the manufacturers.

Appendix A. Supplementary data

Supplementary data associated with this article can be found, in the online version, at https://doi.org/10.1016/j.dental.2018.11.032.

REFERENCES

[1] Mainjot AK, Dupont NM, Oudkerk JC, Dewael TY, Sadoun MJ. From atisanal to CAD-CAM blocks: state of the art of indirect composites. J Dent Res 2016;95:487–95.
[2] Ruse ND, Sadoun MJ. Resin-composite blocks for dental CAD/CAM applications. J Dent Res 2014;93:1232–4.
[3] Lambert H, Durand JC, Jacquot B, Fages M. Dental biomaterials for chairside CAD/CAM: state of the art. J Adv Prosthodont 2017;9:486–95.
[4] Belli R, Wendler M, de Ligny D, Cicconi MR, Petschelt A, Peterlik H, et al. Chairside CAD/CAM materials. Part 1: measurement of elastic constants and microstructural characterization. Dent Mater 2017;33:84–98.
[5] He LH, Swain M. A novel polymer infiltrated ceramic dental material. Dent Mater 2011;27:527–34.
[6] Coldea A, Swain MV, Thiel N. In-vitro strength degradation of dental ceramics and novel PICN material by sharp indentation. J Mech Behav Biomed Mater 2013;26:34–42.
[7] Jun S-K, Kim D-A, Goo H-J, Lee H-H. Investigation of the correlation between the different mechanical properties of resin composites. Dent Mater J 2013;32:48–57.
[8] Fasbinder DJ. Clinical performance of chairside CAD/CAM restorations. J Am Dent Assoc 2006;137(Suppl):22S–31S.
[9] Ilie N, Hilton TJ, Heintze SD, Hickel R, Watts DC, Silikas N, et al. Academy of dental materials guidance—resin composites: Part I—mechanical properties. Dent Mater 2017;33:880–94.
[10] Wendler M, Belli R, Petschelt A, Mevec D, Harrer W, Lube T, et al. Chairside CAD/CAM materials. Part 2: flexural strength testing. Dent Mater 2017;33:99–109.
[11] Awada A, Nathanson D. Mechanical properties of resin-ceramic CAD/CAM restorative materials. J Prosthet Dent 2015;114:587–93.
[12] Lauvahutanon S, Takahashi H, Shiozawa M, Iwasaki N, Asakawa Y, Oki M, et al. Mechanical properties of composite resin blocks for CAD/CAM. Dent Mater J 2014;33:705–10.
[13] Kurtulmus-Yilmaz S, Cengiz E, Ongun S, Karakaya I. The effect of surface treatments on the mechanical and optical behaviors of CAD/CAM restorative materials. J Prosthodont 2018, http://dx.doi.org/10.1111/jopr.12749 [Epub ahead of print].
[14] Lawson NC, Bansal R, Burgess JO. Wear, strength, modulus and hardness of CAD/CAM restorative materials. Dent Mater 2016;32:e275–83.
[15] Drummond JL. Degradation fatigue, and failure of resin dental composite materials. J Dent Res 2008;87:710–9.
[16] Ban S, Anusavice KJ. Influence of test method on failure stress of brittle dental materials. J Dent Res 1990;69:1791–9.
[17] Palin WM, Fleming GJP, Trevor Burke FJ, Marquis PM, Randall RC. The reliability in flexural strength testing of a novel dental composite. J Dent 2003;31:549–57.
[18] Chung SM, Yap AU, Chandra SP, Lim CT. Flexural strength of dental composite restoratives: comparison of biaxial and three-point bending test. J Biomed Mater Res B Appl Biomater 2004;71:278–83.
[19] Börger A, Supancic P, Danzer R. The ball on three balls test for strength testing of brittle discs: stress distribution in the disc. J Euro Ceram Soc 2002;22:1425–36.
[20] With G, Wagemans HHM. Ball-on-ring test revisited. J Am Ceram Soc 1989;72:1538–41.
[21] Shetty DK, Rosenfield AR, McGuire P, Bansal GK, Duckworth WH. Biaxial flexure tests for ceramics. Am Ceram Soc Bull 1980;59:1193–7.
[22] Morena R, Beaudreau GM, Lockwood PE, Evans AL, Fairhurst CW. Fatigue of dental ceramics in a simulated oral environment. J Dent Res 1986;65:993–7.
[23] Zeng K, Oden A, Rowcliffe D. Flexure tests on dental ceramics. Int J Prosthodont 1996;9:434–9.
[24] Higgs WAJ, Lucksanasombool P, Higgs RJED, Swain MV. Evaluating acrylic and glass-ionomer cement strength using the biaxial flexure test. Biomaterials 2001;22:1583–90.
[25] Morrell R. Biaxial flexural strength testing of ceramic materials. In: A national measurement good pactice guide no. 12, NPL; 2007.
[26] Jin J, Takahashi H, Iwasaki N. Effect of test method on flexural strength of recent dental ceramics. Dent Mater J 2004;23:490–6.
[27] Wang Y, Darvell BW. Effect of elastic modulus mismatch on failure behaviour of glass ionomer cement under Hertzian indentation. Dent Mater 2012;28:279–86.
[28] Ona M, Wakabayashi N, Yamazaki T, Takaichi A, Igarashi Y. The influence of elastic modulus mismatch between tooth and post and core restorations on root fracture. Int Endod J 2013;46:47–52.
[29] Park JH, Choi NS. Equivalent Young's modulus of composite resin for simulation of stress during dental restoration. Dent Mater 2017;33:e79–85.
[30] Chung SM, Yap AU, Tsai KT, Yap FL. Elastic modulus of resin-based dental restorative materials: a microindentation approach. J Biomed Mater Res B Appl Biomater 2005;72:246–53.
[31] Masouras K, Silikas N, Watts DC. Correlation of filler content and elastic properties of resin-composites. Dent Mater 2008;24:932–9.
[32] Sabbagh J, Vreven J, Leloup G. Dynamic and static moduli of elasticity of resin-based materials. Dent Mater 2002;18:64–71.
[33] Chabrier F, Lloyd CH, Scrimgeour SN. Measurement at low strain rates of the elastic properties of dental polymeric materials. Dent Mater 1999;15:33–8.
[34] Leone J, Johnson A, Ziada S, Hashemi A, Adili A, de Beer J. Biaxial flexural modulus of antibiotic-impregnated orthopedic bone cement. J Biomed Mater B Appl Biomater 2007;83B:97–104.
[35] Higgs WA, Lucksanasombool P, Higgs RJ, Swain MV. A simple method of determining the modulus of orthopedic bone cement. J Biomed Mater Res 2001;58:188–95.

[36] Braem M, Lambrechts P, Van Doren V, Vanherle G. The impact of composite structure on its elastic response. J Dent Res 1986;65:648–53.
[37] Braem M, Finger W, Van Doren VE, Lambrechts P, Vanherle G. Mechanical properties and filler fraction of dental composites. Dent Mater 1989;5:346–8.
[38] McCormick N, Lord J. Digital image correlation. Mater Today 2010;13:52–4.
[39] Sun Z, Lyons JS, McNeill SR. Measuring microscopic deformations with digital image correlation. Opt Lasers Eng 1997;27:409–28.
[40] Park J, Yoon S, Kwon T-H, Park K. Assessment of speckle-pattern quality in digital image correlation based on gray intensity and speckle morphology. Opt Lasers Eng 2017;91:62–72.
[41] Wang W, Roubier N, Puel G, Allain JM, Infante IC, Attal JP, et al. A new method combining finite element analysis and digital image correlation to assess macroscopic mechanical properties of dentin. Materials 2015;8:535–50.
[42] Palamara JE, Wilson PR, Thomas CD, Messer HH. A new imaging technique for measuring the surface strains applied to dentine. J Dent 2000;28:141–6.
[43] Zhang D, Arola DD. Applications of digital image correlation to biological tissues. J Biomed Opt 2004;9:691–9.
[44] Lau A, Li J, Heo YC, Fok A. A study of polymerization shrinkage kinetics using digital image correlation. Dent Mater 2015;31:391–8.
[45] Li J, Fok AS, Satterthwaite J, Watts DC. Measurement of the full-field polymerization shrinkage and depth of cure of dental composites using digital image correlation. Dent Mater 2009;25:582–8.
[46] Lee H-H, Lee J-H, Yang T-H, Kim Y-J, Kim S-C, Kim G-R, et al. Evaluation of the flexural mechanical properties of various thermoplastic denture base polymers. Dent Mater J 2018, http://dx.doi.org/10.4012/dmj.2017-373.
[47] Huang CW, Hsueh CH. Piston-on-three-ball versus piston-on-ring in evaluating the biaxial strength of dental ceramics. Dent Mater 2011;27:e117–23.
[48] Kirstein AF, Woolley RM. Symmetrical bending of thin circular elastic plates on equally spaced point supports. J Res Natl Bur Stand 1967;71C:1–10.
[49] Chae S-H, Zhao J-H, Edwards D, Ho P. Verification of ball-on-ring test using finite element analysis. Proceedings of the 12th IEEE Intersociety Conference 2010:1–6.
[50] Westergaard HM. Stresses in concrete pavements computed by theoretical analysis. Public Roads 1926;7:25–35.
[51] Quinn JB, Quinn GD. A practical and systematic review of Weibull statistics for reporting strengths of dental materials. Dent Mater 2010;26:135–47.
[52] Cheng P, Sutton MA, Schreier HW, McNeill SR. Full-field speckle pattern image correlation with B-Spline deformation function. Exp Mech 2002;42:344–52.
[53] Alander P, Lassila LVJ, Vallittu PK. The span length and cross-sectional design affect values of strength. Dent Mater 2005;21:347–53.
[54] Sakaguchi RL, Powers JM. Fundamentals of matrials scienc. In: Craig's restorative dental materials. 13th ed. Elsevier; 2012. p. 34–81.
[55] Lim K, Yap AU-J, Agarwalla SV, Tan KB-C, Rosa V. Reliability, failure probability, and strength of resin-based materials for CAD/CAM restorations. J Appl Oral Sci 2016;24:447–52.
[56] Harrer W, Morrell R, Danzer R. Fractography of biaxial tested Si3N4-specimens. J Eur Ceram Soc 2014;34:3283–9.
[57] ASTM F394-78 (Reappproved 1996). Standard test method for biaxial flexure strength (modulus of rupture) of ceramic substrates (Withdrawn 2001). PA, USA: ASTM Inernational; 1996.
[58] Kao R, Perrone N, Capps W. Large-deflection solution of the coaxial-ring-circular-glass-plate flexure problem. J Am Ceram Soc 1971;54:566–71.
[59] Lee KH, Rhee SH. The mechanical properties and bioactivity of poly(methyl methacrylate)/SiO(2)-CaO nanocomposite. Biomaterials 2009;30:3444–9.
[60] Miura D, Miyasaka T, Aoki H, Aoyagi Y, Ishida Y. Correlations among bending test methods for dental hard resins. Dent Mater J 2017;36:491–6.
[61] Pick B, Meira JB, Driemeier L, Braga RR. A critical view on biaxial and short-beam uniaxial flexural strength tests applied to resin composites using Weibull, fractographic and finite element analyses. Dent Mater 2010;26:83–90.
[62] Chao L-Y, Shetty DK. Reliability analysis of structural ceramics subjected to biaxial flexure. J Am Ceram Soc 1991;74:333–44.
[63] Shetty DK, Rosenfield AR, Duckworth WH, Held PR. A biaxial-flexure test for evaluating ceramic strengths. J Am Ceram Soc 1983;66:36–42.
[64] Frandsen HL. Weibull statistics effective area and volume in the ball-on-ring testing method. Mech Mater 2014;73:28–37.
[65] Harrer W, Danzer R, Supancic P, Lube T. The ball on three balls test: strength testing of specimens of different sizes and geometries. Proceedings of the 10th International Conference of the European Ceramic Society 2007:1271–5.
[66] Breder K, Andersson T, Schölin K. Fracture strength of α- and β-SiAlON measured by biaxial and four-point bending. J Am Ceram Soc 1990;73:2128–30.
[67] Kalidindi S, Abusafieh A, El-Danafa E. Accurate characterization of machine compliance for simple compression testing. Exp Mech 1997:37.
[68] Siddiqui MZ, Tariq F, Naz N, Ahmed M. Determination of Young's modulus of metallic and composite materials by digital image correlation. J Space Technol 2012;1:32–7.
[69] Atkinson A, Bastid P, Liu Q. Mechanical properties of magnesia–spinel composites. J Am Ceram Soc 2007;90:2489–96.